"Ship-in-Bottle" Catalyst Technology

NOVEL TEMPLATING FABRICATION OF PLATINUM GROUP METALS NANOPARTICLES AND WIRES IN MICRO/MESOPORES

By Masaru Ichikawa

Catalysis Research Center, Hokkaido University, Sapporo, Japan

The fabrication of nanostructured materials, such as nanometre-sized particles and wires, which are potential building blocks for tailored metal catalysts and electronic devices, is a major challenge currently being investigated. During the last ten years, "ship-in-bottle" catalyst technology using zeolitic crystals as microsized reactors for the template fabrication of metal clusters, nanoparticles and wires has been developed. This novel technology for cluster manipulation gives an ordered basis for better control of particle size, metal compositions and morphology. A variety of platinum metals carbonyl clusters has been synthesised, extracted and characterised, and transformed into nanoparticles and nanowires encapsulated in micro/mesoporous cavities and channels. The resulting nanostructured platinum metals exhibit higher catalytic performances and stabilities for various catalytic reactions as well as having unique magnetic properties, compared with conventional metals. An overview of this technology and recent developments resulting in excellent catalyst performances are described.

Platinum group metals are widely used in commercial catalysts for the petrochemical industries (oil refinery, fine chemicals and oxo processes), for controlling vehicle emissions (three-way and deNOx) and in fuel cells (PEM/SPE and PAFC). Their catalytic performances depend on the state of metal dispersion (measured by particle sizes and distribution), their structure (shape and morphology), the metal compositions (indicated by geometric and spatial spectra), and the metal-support interactions (such as between metal oxides and carbon). The dispersion and the morphology of the platinum metals and their alloys can be controlled by the correct selection of the metal precursors and the supporting materials and by the method of preparation. The conventional preparation of catalysts is based on prior knowledge to control the complex inorganic reactions of the metallic salts – their impregnation, calcination and reduction. However, such catalyst technology is not rigorous enough in some instances to produce catalysts with optimum performances and stabilities for industrial processes.

During the last decades, pioneering work to

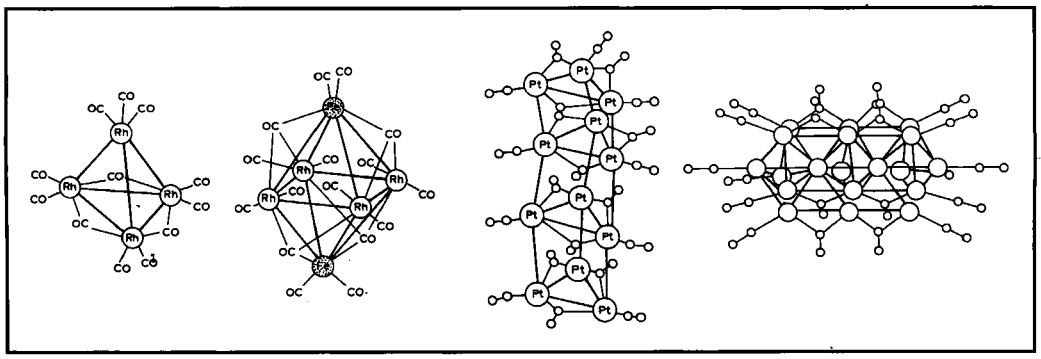

Fig. 1 Some platinum metals clusters used as molecular precursors for tailored metal catalysts, from the left: $Rh_4(CO)_{12}$, $[Fe_2Rh_4(CO)_{16}]^{2-}$, $[Pt_{12}(CO)_{24}]^{2-}$ and $[Pt_{19}(CO)_{22}]^{4-}$

Table I

Typical Cages and Channels with Molecular Dimensions

Material	Pore type	Pore size, Å, (nm)	Notes
Zeolite: faujasite NaY	Micropore	12 (1.2)	3D chamber, SiO_2:Al_2O_3 = 5.6
Zeolite: faujasite NaX	Micropore	12	SiO_2:Al_2O_3 = 3.2
Zeolite: ALPO-5	Micropore	6 (0.6)	One dimensional channel
Mesoporous sieve materials: FSM-16	Mesopore	28 (2.8)	Hexagonal ordered channels
FSM-16	Mesopore	48 (4.8)	Hexagonal ordered channels

develop tailor-made catalysts has been undertaken using molecular precursors, such as metal clusters, grafted onto metal oxide supports for better control of the catalyst, see Figure 1 (1–4). The relevant chemistry, characterisation and catalytic performances of surface-grafted metal clusters has been extensively reviewed by Gates (1), Basset (2) and Ichikawa (3). More recently, the microsized cavities and channels of porous materials, such as zeolites and layered clays, have been proposed as the "ultimate reaction vessel" to synthesise metal clusers by templating (3, 5, 6). (These reactions can also be carried out in solution, but do not proceed selectively.) This has been called the "ship-in-bottle" synthesis, being the molecular analogy of the tricky construction of a model ship from its component parts inside a whisky bottle! With this new nanotechnology, metal clusters can be uniformly prepared and sufficiently accommodated in each micro/mesopore and channel to prevent facile migration and cluster-sintering under the prevailing preparative and reaction conditions.

Recent progress of "ship-in-bottle" catalyst technology, including the template synthesis, characterisation and catalysis by metal clusters encapsulated in micro/mesoporous space is reviewed here. This is important for establishing a "rational" design for nanomaterials (robust clusters, nanoparticles, nanoalloys and nanowires of platinum metals) for use in both tailored metal catalysts and electronic/magnetic devices (7).

"Ship-in-Bottle" Platinum Metals Clusters in NaY Micropores

Zeolites, namely faujasites (NaY, NaX), mordenite, ZSM-5 and ALPO-5, are aluminosilicate and aluminophosphate crystals consisting of microporous cages and channels of molecular dimensions (5 to 12 Å), see Table I, interconnected by smaller windows, see Figure 2.

Such micropores and ordered channels can be regarded as "nanometre-sized microreactors", offering a templating space for the synthesis of selected metal complexes, such as platinum metals clusters. While some robust metal carbonyl clusters, such as $Rh_6(CO)_{16}$ (van der Waal radius of 10 Å) and $[Pt_{12}(CO)_{24}]^{2-}$ (8 × 12 Å) are unable to enter directly into the NaY (12 Å) pores through the small window (6 Å), they can, however, be synthesised and encapsulated in the cages by successive

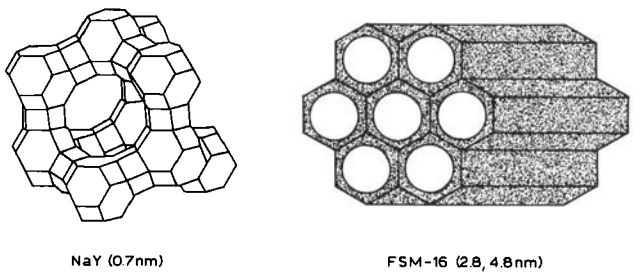

Fig. 2 Some examples of micro- and mesoporous materials, NaY and FSM-16, used as templating microreactors for "ship-in-bottle" synthesis of platinum metals clusters, nanoparticles and wires

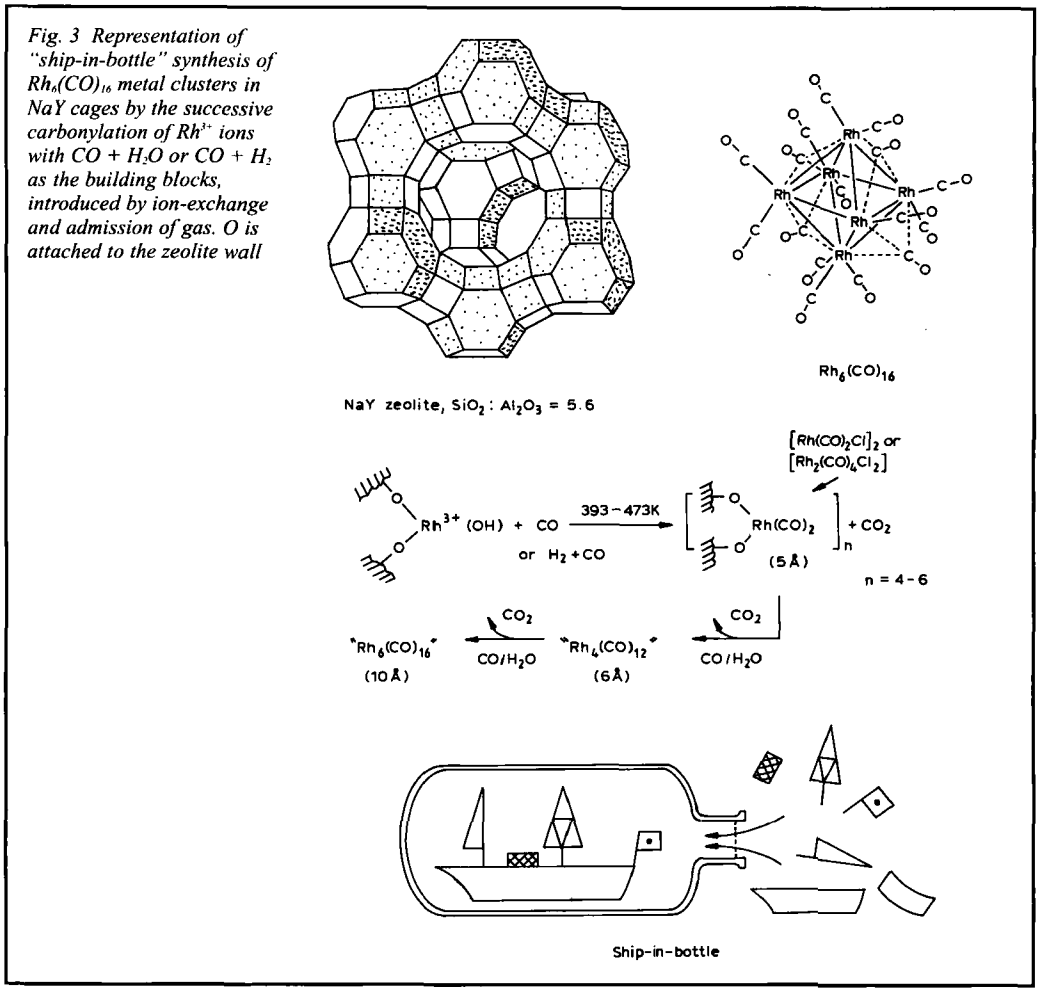

Fig. 3 Representation of "ship-in-bottle" synthesis of $Rh_6(CO)_{16}$ metal clusters in NaY cages by the successive carbonylation of Rh^{3+} ions with CO + H_2O or CO + H_2 as the building blocks, introduced by ion-exchange and admission of gas. O is attached to the zeolite wall

carbonylation reactions of the precursor rhodium and platinum ions with CO + H_2 or CO + H_2O, which act as building blocks, entering through the window. The metal ions are introduced into the cages by conventional ion-exchange, while some volatile subcarbonyls and metal complexes are introduced into the cages by the solid-state dispersion technique (8). This *in situ* intrazeolitic preparation of nanomaterials, in this case $Rh_6(CO)_{16}$ and $[Pt_{12}(CO)_{24}]^{2-}$ in micropores, is the "ship-in-bottle" synthesis, see Figure 3.

To produce $Rh_6(CO)_{16}$ in NaY, ion-exchanged Rh^{3+} in NaY zeolite was reduced with CO + H_2 or CO + H_2O at 393 to 473 K to give the mononuclear dicarbonyl species, $[Rh(CO)_2(-O-)_2]$ in Figure 3, where O are shared with the zeolite wall. This then migrated through the zeolite channels and underwent a subsequent cluster-oligomerisation to $Rh_4(CO)_{12}$ (6 Å) and $Rh_6(CO)_{16}$ (10 Å), the latter just fitting in the interior of NaY (12 Å) (9, 10). This is analogous chemistry to that occurring in aqueous alkaline solution (11). $Rh_6(CO)_{16}$ was selectively produced with a minor contribution from residual mononuclear Rh carbonyls inside NaY. $Rh_6(CO)_{16}$ encapsulated in a NaY zeolite cage by the "ship-in-bottle" technique was well characterised by IR bands for linear and face-bridging carbonyls, which are different from those of $Rh_6(CO)_{16}$ adsorbed on NaY surfaces. Additionally, EXAFS (Extended X-ray Absorption Fine Structure) data provided evidence for the stoichiometric formation of a hexanuclear rhodium carbonyl cluster, in good

Table II

Platinum Metal Clusters in Micro/Mesopores, Prepared by the "Ship-in-bottle" Technique

Platinum metals clusters*/pore diameter	IR bands (ν_{CO}, cm^{-1}) (linear, bridging)	Precursor/pores (reaction) for "ship-in-bottle" synthesis
$[Rh_4(CO)_{12}]$/ALPO-5 (6 Å) $[Rh_6(CO)_{16}]$/NaY (12 Å)	2082s, 1832m (edge) 2097s, 2066w, 1760s	$Rh_2(CO)_4Cl_2$/ALPO-5 (CO + H_2) Rh^{3+}/NaY (CO + H_2)
$[Ir_6(CO)_{16}]$/NaY $[Ir_6(CO)_{16}]$/NaY	2095s, 2048m, 1744m 2082s, 2040m, 1816m, 1730m	Ir^{4+}/NaY (CO + H_2) $Ir(CO)_2$(acac)/NaY (CO + H_2)
$[HRu_6(CO)_{18}]^-$/NaY $[Ru_6(CO)_{18}]^{2-}$/NaX (12 Å)	2126w, 2062s, 2044w, 1975m 2000w, 1972w, 1925m, 1743m	$[Ru(NH_3)_4]^{2+}$/NaY (CO + H_2) $[Ru(NH_3)_4]^{2+}$/NaX (CO + H_2)
$[Pt_3(CO)_3(\mu_2\text{-}CO)_3]$/NaY (12 Å) $[Pt_9(CO)_{18}]^{2-}$/NaY $[Pt_{12}(CO)_{24}]^{2-}$/NaY $[Pt_{15}(CO)_{30}]^{2-}$/FSM-16 (28 Å) $[Pt_{18}(CO)_{36}]^{2-}$/FSM-16 (48 Å)	2112s, 1896m, 1841m 2056s, 1798m 2080s, 1824m 2086s, 1882m 2065s, 1878m	Pt^{2+}/NaY (CO + H_2O) at 323 K Pt^{2+}/NaY (CO + H_2O) at 343 K $[Pt(NH_3)_4]^{2+}$/NaY (CO + H_2) at 393 K H_2PtCl_6/FSM-16 (CO + H_2O) H_2PtCl_6/FSM-16 (CO + H_2O)
$[Rh_{6-x}Ir_x(CO)_{16}]$/NaY (x = 2, 3, 4)	2098s, 2060m, (1756–1744)m	$[(6–x)Rh^{3+} + xIr^{4+}]$/NaY (CO + H_2) (x = 2–4)
$[Fe_2Rh_4(CO)_{15}]^{2-}$/NaY	2078s, 2020m, 1980m, 1744w, 811m	$[HFe_3(CO)_{11}]^-$/NaY ($Rh_4(CO)_{12}$)
$[HRuCo_3(CO)_{12}]$/NaY	2084s, 2064m, 1989m,1812m	Ru^{3+}/NaY ($Co_2(CO)_8$ + CO/H_2)

* *The metal clusters in pores have been characterised by IR, EXAFS, UV-vis spectroscopies*
s = strong, m = medium, w = weak

agreement with a free molecule, in terms of coordination numbers and atomic distance.

Similarly, $Ir_6(CO)_{16}$ in NaY cages was synthesised using ion-exchanged Ir^{4+}/NaY with CO + H_2 at 1 atm and 323 K via the intermediate formation of $Ir(CO)_2$ and $Ir_4(CO)_{12}$, in analogous processes to those for $[Rh_6(CO)_{16}]$/NaY (9, 12). Gates and colleagues reported that $Ir(CO)_2$(acac) impregnated with NaY was converted, using CO + H_2 at 20 atm and 623 K, to $Ir_6(CO)_{16}$, whereas $[Ir_6(CO)_{15}]^{2-}$ was formed in basic NaX (SiO_2:Al_2O_3 = 3.2) (13). In this case, the zeolite micropores acted as a "common templating microreactor" to selectively synthesise the homologous hexanuclear clusters in the confined reaction space.

Sachtler and co-workers reported a new type of palladium carbonyl cluster $[Pd_{13}(CO)_x]$ (x is unknown) in the supercage of a NaY zeolite (12 Å) and $[Pd_6(CO)_x]$ in a NaA zeolite (5 Å), although they were not fully characterised by IR and EXAFS (14). Ichikawa and colleagues have recently extended the "ship-in-bottle" synthesis to some other metal clusters, such as $H_4Ru_4(CO)_{12}$/NaY (15), $[HRu_6(CO)_{18}]^-$/NaY (16), $[Ru_6(CO)_{18}]^{2-}$/NaX (17), $[Pt_9(CO)_{18}]^{2-}$/NaY (18, 19) and $[Pt_{12}(CO)_{24}]^{2-}$/NaY (20). In particular, to produce $[Pt_{12}(CO)_{24}]^{2-}$/NaY, calcined Pt^{2+}/NaY was heated from 298 to 373 K under CO with a trace of H_2O. This resulted in the successive formation of different carbonyl species with characteristic carbonyl IR bands. By analogy with IR data from known platinum carbonyl complexes, it was suggested that Pt^{2+}/NaY reacts with CO to form PtO(CO) in NaY and a proposed Pt trigonal intermediate species $[Pt_3(CO)_3(\mu_2\text{-}CO)_3]$. These are eventually converted, by stacking, to the dark-green Chini complex of $[Pt_{12}(CO)_{24}]^{2-}$ (2080s and 1824m cm^{-1}) (20).

By contrast, $[Pt(NH_3)_4]^{2+}$ ion-exchanged with NaY selectively gave the smaller, orange-brown Chini cluster, $[Pt_9(CO)_{18}]^{2-}$, which has intense IR bands at 2056s and 1798m cm^{-1} (19, 20).

The spatial restrictions of the micropores in NaY and NaX may hinder cluster migration and interactions, and promote cluster isolation and

stability. "Ship-in-bottle" syntheses may provide opportunities for the "rational" design of discrete platinum metals clusters of uniform size and metal composition. Clusters already made have sufficient stability against sintering and leaching under prevailing reaction conditions. Some encapsulated metal clusters are listed in Table II.

Robust Platinum Clusters in the Channels of Mesoporous FSM-16

A new family of mesoporous sieve materials, such as FSM-16 and MCM-41, has been synthesised by using micelle surfactant templates, such as alkyltrimethyl ammonium salts (21, 22). These materials consist of ordered mesoporous channels of diameter 20 to 100 Å, larger than those of conventional zeolites. The mesoporous sieve materials are potential hosts for robust metal clusters aligned in the ordered channels and accessible to larger substrates in catalytic reactions.

Chini Cluster Synthesis

Robust rod-like platinum clusters $[Pt_3(CO)_6]_n^{2-}$ n = 5 and 6; 6 × 15 to 18 Å) (the Chini complex) have been successfully synthesised using the mesoporous FSM-16 channels (28 and 48 Å) as a host reactor (23, 24). This was achieved by exposing FSM-16 (28 Å) impregnated with H_2PtCl_6 to CO at 323 K (22) and gave *cis*-$Pt(CO)_2Cl_2$ and $[Pt(CO)Cl_3]^-$. These were then converted with CO + H_2O vapour at 323 K to an olive-green complex (23). The Chini complex extracted from FSM-16 by cation metathesis was identified as $[Pt_{15}(CO)_{30}]^{2-}$ by FTIR and UV-vis spectroscopy (ν_{CO} = 2086s and 1882m cm^{-1} and UV-vis reflectance at λ_{max} = 452 and 805 nm). The Pt_{15} cluster anions formed in FSM-16 were isolated and relatively stabilised by using quaternary alkyl ammonium cations NR_4^+ as spacing molecules.

Similarly, a larger trigonal prismatic Pt_{18} cluster anion has been synthesised uniformly (24, 29) by the reductive carbonylation of H_2PtCl_6 in FSM-16 of channel size 48 Å. This was characterised by IR, UV and EXAFS spectroscopy by analogy to the reference complex, $[NEt_4]_2[Pt_3(CO)_6]_6$.

The average interfacial distances ($R_{(Pt\text{-}Pt)}$ = 3.07 Å) between adjacent triplatinum planes for these clusters in FSM-16, that is $[Pt_3(CO)_6]_5^{2-}/NEt_4Cl/$ FSM-16 (28 Å) and $[Pt_3(CO)_6]_6^{2-}/NEt_4Cl/FSM\text{-}16$ (48 Å), are in good agreement with those of the reference salt $[NEt_4]_2[Pt_3(CO)_6]_5$ in boron nitride, within experimental error. By contrast, for Chini clusters in NaY micropores, for example, $[Pt_3(CO)_6]_4^{2-}/NaY$ and $[Pt_3(CO)_6]_3^{2-}/NaY$ (19, 20) the interfacial Pt-Pt distance of the Pt_3 and Pt_{12} triangle is substantially shorter ($R_{(Pt\text{-}Pt)}$ = 2.98 to 2.99 Å) than the reference compounds both in crystalline form and in solution. This is because of compression and distortion of the bulky Chini clusters by the small (12 Å) NaY (and NaX) microcavities. Transmission electron microscopy (TEM) observation of $[Pt_3(CO)_6]_5^{2-}/FSM\text{-}16$ revealed that the platinum clusters were small specks of size 10 to 15 Å, uniformly scattered and aligned in the ordered FSM-16 channels (21, 22). No larger platinum particles or crystals were found on the external surface of FSM-16.

Alloy Clusters in NaY and MCM-41 Cages

Bimetallic carbonyl clusters, $Rh_{6-x}Ir_x(CO)_{16}/$ NaY (x = 2–4) (9–12), $[Fe_2Rh_4(CO)_{15}]^{2-}/NaY$ (25) and $[HRuCo_3(CO)_{12}]/NaY$ (17) have been synthesised by the "ship-in-bottle" technique and characterised by IR, EXAFS, UV and Raman spectroscopy, see Table II.

A series of $[Rh_{6-x}Ir_x(CO)_{16}]/NaY$ (x = 2–4) clusters was prepared by reductive carbonylation of double ion-exchanged $[Rh^{3+} + xIr^{4+}]/NaY$ in CO + H_2 at 1 atm and 393 to 473 K, in the same way as $[Rh_6(CO)_{16}]/NaY$ (9, 10) and $[Ir_6(CO)_{16}]/NaY$ (9, 12) were prepared. These had linear and face-bridging CO bands characteristic of hexanuclear metal clusters. EXAFS studies revealed that the formation of the bimetallic RhIr clusters was stoichiometric, with metal compositions similar to those of the starting ion-exchanged NaY. The reduced alloy clusters $Rh_{6-x}Ir_x/NaY$ (x = 2–4) were prepared by oxidising the carbonyl clusters, followed by reduction with hydrogen at 673–723 K. This novel preparation of hexanuclear RhIr alloy clusters encapsulated in NaY is shown in Figure 4.

The RhFe carbonyl cluster $[Fe_2Rh_4(CO)_{15}]^{2-}$ has also been prepared by the solid-state reaction of

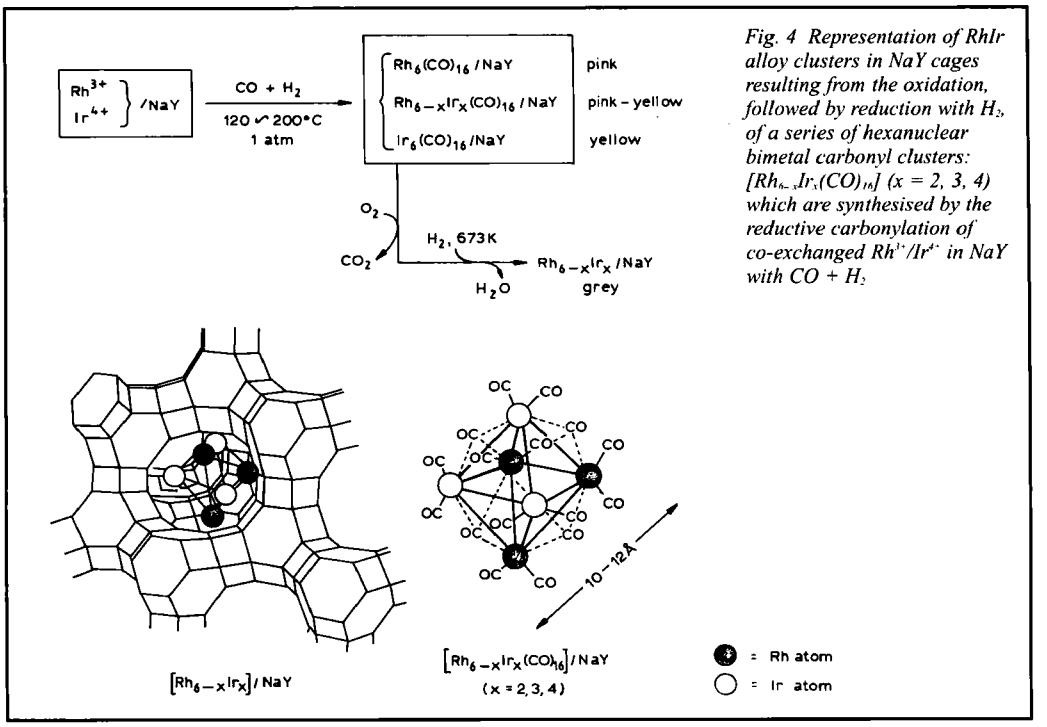

Fig. 4 Representation of RhIr alloy clusters in NaY cages resulting from the oxidation, followed by reduction with H_2, of a series of hexanuclear bimetal carbonyl clusters: $[Rh_{6-x}Ir_x(CO)_{16}]$ (x = 2, 3, 4) which are synthesised by the reductive carbonylation of co-exchanged Rh^{3+}/Ir^{4+} in NaY with CO + H_2

$[HFe(CO)_{11}]$/NaY with $Rh_4(CO)_{12}$ at 343 K (25), in an analogous reaction to that in solution between $[Fe_3(CO)_{11}]^{2-}$ and $Rh_4(CO)_{12}$ or $Rh_2(CO)_4Cl_2$. An IR study revealed that the active $Rh(CO)_2$ species, generated by decomposition of precursor $Rh_4(CO)_{12}$, migrates inside the NaY zeolite framework.

This facile migration of monometal carbonyls results in the rebuilding of more stable bimetallic cluster anions. However, groups lead by Thomas and Johnson recently reported an elegant example of loading giant bimetal clusters, such as $[Ru_{12}C_2(CO)_{16}Cu_4Cl_2]^{2-}$ and $[Ag_3Ru_{10}C_2(CO)_{28}Cl]^{2-}$, as the precursors in mesopores of MCM-41 (28 Å) (26). TEM and EXAFS data showed no evidence of segregation or aggregation after the pyrolysis of the RuCu and AgRu precursor clusters in MCM-41.

The bimetal catalysts produced are ~ 15 Å in diameter, rosette-shaped with twelve exposed ruthenium atoms connected to a square base composed of partly concealed copper atoms. These RuCu clusters are anchored by copper ions bound to four oxygen bridging silanols of the mesopore lining. This anchoring model for RuCu clusters on MCM-41 is analogous to that for RhFe and RuCo bimetal clusters on silica, encapsulated in NaY cages (27), and immobilised by Fe-O and Co-O bonds, respectively, attached to silica or alumina surfaces.

Cluster Transformations to Nanoparticles in Micro/Mesopores

After the mild oxidation of $[Rh_6(CO)_{16}]$/NaY with dry O_2 by heating from 293 to 473 K, IR and EXAFS data suggest that the Rh carbonyl cluster is decomposed and converted to an oxide cluster. By successive reductions with hydrogen at 473 and 673 K, a skeletal rhodium cluster formed in the cavity (11). EXAFS analysis showed that the rhodium hexanuclear atomic unit had been retained in the zerovalent state. The coordination number (C.N.) is the same (C.N. = 3.2) as the original $[Rh_6(CO)_{16}]$/NaY and the atomic distances are close to those of metallic rhodium ($R_{(Rh\text{-}Rh)}$ = 2.72 Å). Exposure of this reduced rhodium, Rh_6, to CO at 300 K results in the stoichiometric formation ($CO{:}Rh_{(total)}$ = 2.6) of $Rh_6(CO)_{16}$. Thus the NaY micropores provide the preparative and catalytic cages to accommodate the metal clusters through cyclic sequences of oxidation, reduction with H_2

and carbonylation with CO/H_2 to prevent cluster sintering in the micropores at higher temperatures.

Robust platinum clusters, such as $[Pt_{15}(CO)_{30}]^{2-}$ in FSM-16 (28 Å) and $[Pt_{18}(CO)_{36}]^{2-}$ in FSM-16 (48 Å) are similarly transformed to nanoparticles by gentle heating at 300 to 473 K in vacuum and were characterised by EXAFS and FTIR (27, 33). The platinum nanoparticles (size 15 to 20 Å), see Figure 5, were uniformly positioned, aligned and synthesised in the ordered mesoporous channels of FSM-16 by thermal evacuation at 573 K to remove CO from $[Pt_{15}(CO)_{30}]^{2-}$ in FSM-16. The channels thus play a templating role in the synthesis of platinum metal nanoparticles by thermal pyrolysis of the Chini platinum complexes, see Figure 6.

Platinum Nanowires in Mesoporous Channels of FSM-16

We have recently reported the templated fabrication of platinum nanowires in mesoporous FSM-16 channels by the photoreduction of

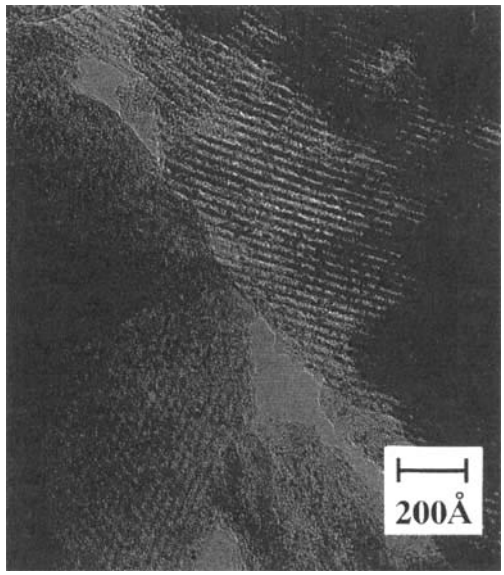

Fig. 5 TEM of platinum nanoparticles (diameter 15 to 20 Å) prepared by controlled removal of CO at 573 K for 5 hours from Chini cluster anions, $[Pt_3(CO)_6]_5^{2-}$, synthesised in FSM-16. The particles are uniformly aligned in the ordered FSM-16 (28 Å) channels

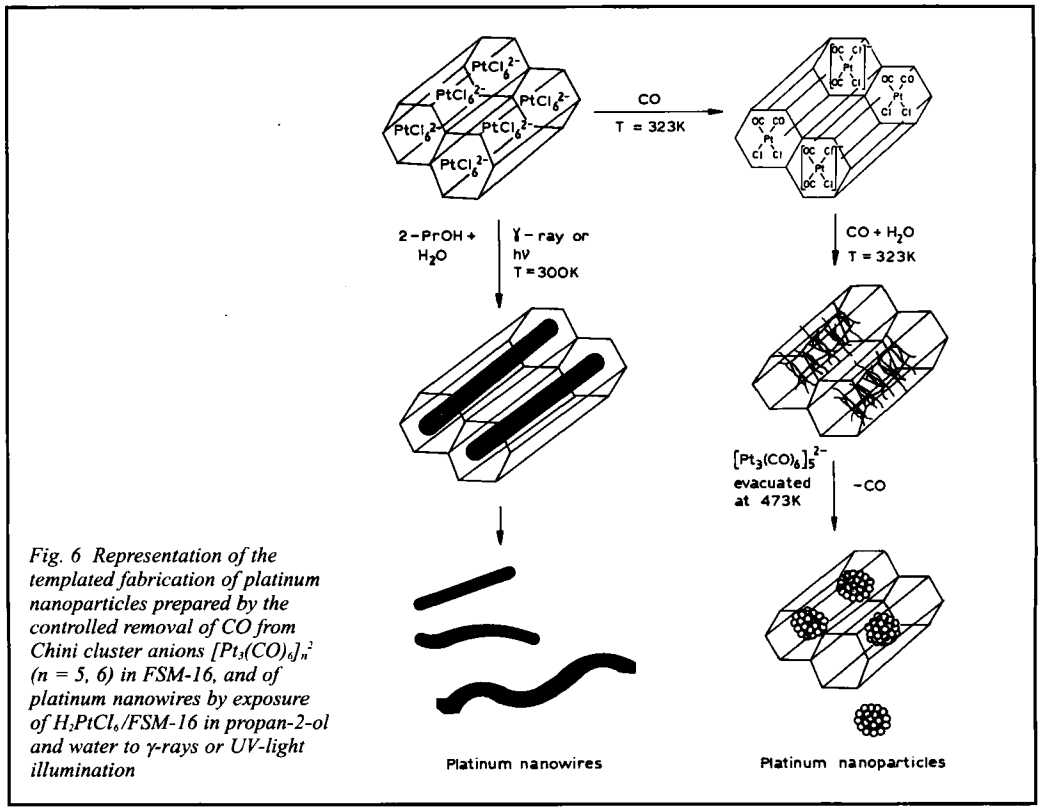

Fig. 6 Representation of the templated fabrication of platinum nanoparticles prepared by the controlled removal of CO from Chini cluster anions $[Pt_3(CO)_6]_n^{2-}$ (n = 5, 6) in FSM-16, and of platinum nanowires by exposure of H_2PtCl_6/FSM-16 in propan-2-ol and water to γ-rays or UV-light illumination

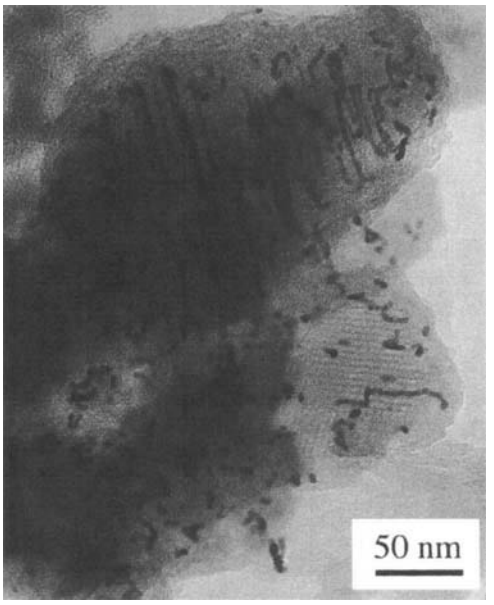

Fig. 7 TEM of platinum nanowires in FSM-16 prepared by the reduction of H_2PtCl_6/FSM-16 with propan-2-ol and water by γ-ray irradiation at 300 K for 5 hours. The nanostructured wires (3 nm × 50–200 nm long) are clearly aligned in the ordered channels of FSM-16 (28 Å)

H_2PtCl_6/FSM-16 in the presence of propan-2-ol and water (28, 29). A typical TEM image of platinum nanowires in FSM-16 (28 Å) is shown in Figure 7. The nanowires have diameters of ~ 3 nm, which is the pore size of FSM-16; their lengths can range from 50 to 200 nm. The nanowires are in the internal channels of FSM-16, not on the external surface. The TEM also shows that the nanowires have crystal faces, and the high resolution electron diffraction image gives a clear fringe pattern of Pt(110), implying that the platinum wires consist of a single crystal phase. The mesoporous channels of the FSM-16 thus act as a template to fabricate the platinum nanowires by a one-dimensional elongation of platinum crystals, see Figure 6. EXAFS characterisation shows that the platinum nanowires and nanoparticles in FSM-16 have different parameters to platinum foils. For nanowires, the Pt-Pt distance and coordination number are 0.274 nm and 7.8, respectively, but 0.272 nm and 6.7, respectively, for nanoparticles (29).

However, XANES (X-ray Absorption Near Edge Structure) and XPS indicate that the nanowires in FSM-16 are slightly electron-deficient compared with platinum foil and nanoparticles in FSM-16. This may be due to the dominant interaction of the nanowires with the inner acidic surface of the FSM-16 pores. On exposure to UV-light, TEM and EXAFS studies show that platinum nanoparticles (~ 1 to 2 nm diameter) are initially formed by the photoreduction of the platinum cations impregnated in the mesopores. $[PtCl_6]^{2-}$ ions then migrate to the vicinity of the nanoparticles and are reduced on their surfaces to grow and elongate as nanowires in the confined FSM-16 channels, see Figure 8.

Ryoo has also reported the thermal preparation of platinum nanowires in MCM-41 by a stepwise hydrogen reduction of platinum ions which add to pre-reduced Pt/MCM-41 at above 823 K (30).

Magnetic susceptibility measurements on samples of platinum nanowires and nanoparticles of ~ 2 nm size encapsulated in FSM-16 were performed by varying the temperature from 5 to 300 K at 30 kOe using a SQUID magnetometer (28). The inverse susceptibility of the platinum nanoparticle/FSM-16 was found to obey the Curie-Weiss law with magnetisation ~ 1.54 μ_b/gram of Pt and Curie temperature, θ = 0.05 K, see Figure 9. By contrast, for platinum nanowire/FSM-16, below 100 K, a Curie-Weiss law dependency was observed with magnetisation ~ 0.131 μ_b/gram of Pt, and Curie temperature, θ = 0.48 K. There is a clear deviation from the Curie-Weiss law above 100 K. This unique superpara-like magnetism of the platinum nanowire/FSM-16 can be explained by the quantum size effect or spin-ordering due to the one-dimensional morphology characteristic of a nanowire, and may be based on a quantum confinement effect in the narrow wire and hetero-coupling between internal mesoporous channels of FSM-16.

Separating the platinum nanowires from the FSM-16 was attempted by dissolving FSM-16 with aqueous HF or NaOH solution, but the nanowires decomposed to form platinum aggregates. The platinum nanowires were successfully extracted when $[NBu_4]Cl$ in a benzene/ethanol solution was used. TEM-EDX showed that the nanowires were pure platinum with no silicon, indicating successful

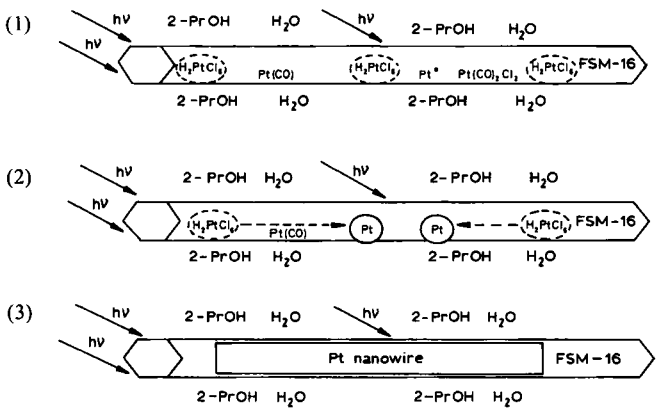

Fig. 8 The growth mechanism of platinum nanowires: (1) photoreduction of $[PtCl_6]^{2-}$ ions to platinum nanoparticles in the ordered mesoporous channels of FSM-16 and (2) $[PtCl_6]^{2-}$ ions and platinum carbonyl species migrate to the vicinity of the preformed nanoparticles, where they are reduced on the nanoparticle surfaces, to grow and elongate as: (3) nanowires in the FSM-16

removal from the FSM-16 support. The extracted wires are probably stabilised by the $[NBu_4]Cl$ which covers their surface to form organosols.

Catalytic Reactions

The catalytic performances of encapsulated platinum nanomaterials have been investigated as functions of their morphology, structural confinement and cluster-support interactions.

Water Gas Shift Reaction

The water gas shift reaction (WGSR) has been recently studied on $[Pt_{15}(CO)_{30}]^{2-}/[Et_4N]^+$/FSM-16 (23), platinum nanoparticles/FSM-16 (28 Å) (24), platinum nanowires/FSM-16 (28, 29), $[Pt_{12}(CO)_{24}]^{2-}$/NaY and on $[Pt_9(CO)_{18}]^{2-}$/NaY (12 Å) (31).

As shown in Table III, $[Pt_{15}(CO)_{30}]^{2-}$ cluster anions in FSM-16 exhibited remarkably high activities to form an equimolar mixture of CO_2 and H_2 at 298 to 323 K, compared to the Pt_{12} and Pt_9 cluster anions in NaY. The higher activity of the Pt_{15} cluster anions in FSM-16 is probably due to the flexible cluster frameworks, similarly seen in solution, compared with the Pt_{12} and Pt_9 clusters confined in the NaY micropores. The turnover rates (TOF: mol(CO_2)/Pt surface atom/min) for the WGSR at 323 K for platinum nanowires (2.8 nm × 100–200 nm long)/FSM-16 (28 Å), were 60

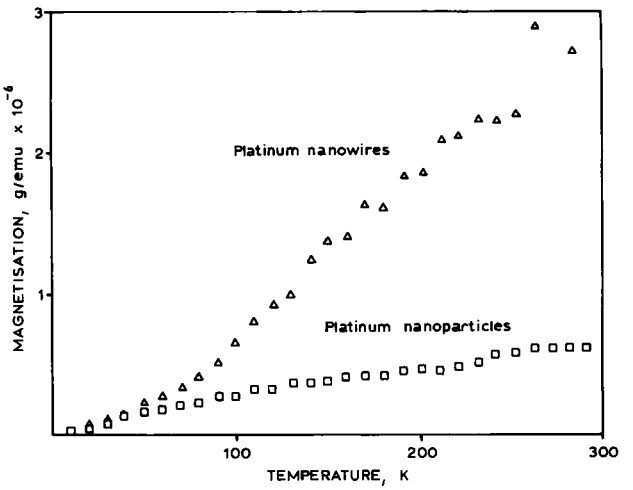

Fig. 9 Temperature dependence of 1/χ (magnetisation) for a sample of platinum nanoparticles and a sample of platinum nanowire both in FSM-16 (2.8 nm) and prepared by the photoreduction of H_2PtCl_6/FSM-16 with propan-2-ol + CO under γ-ray irradiation at 300 K for 5 hours. All the samples were measured at 5 to 300 K and 30 kOe

Table III

Water Gas Shift Reaction on Platinum Carbonyls, Platinum Nanowires, Platinum Nanoparticles and Platinum, Encapsulated in FSM-16, Zeolites and on Alumina

Platinum catalyst	WGSR ($CO + H_2O \rightarrow CO_2 + H_2$), k min^{-1} (323 K)[a] × 10^{-3}	Activation energy, kJ mol^{-1}
$[Pt_{15}(CO)_{30}]^{2-}[NEt_4]^+$/FSM-16 (2.8 nm)	60	28
$[Pt_{15}(CO)_{30}]^{2-}[NBu_4]^+$/FSM-16 (2.8 nm)	23	ND
$[Pt_{12}(CO)_{24}]^{2-}$/NaY (1.3 nm)	2.1	ND
$[Pt_9(CO)_{18}]^{2-}$/NaY (1.3 nm)	3.8	40
Pt nanowire/FSM-16 (2.8 nm)	110	20
Pt nanoparticle/FSM-16 (2.8 nm)	1.3	48
Pt/γ-Al_2O_3[b]	0.1	ND

[a] *CO (200 torr) + H_2O (15 torr); TOF: (mol(CO_2)/Pt surface atom/min). The Pt surface is estimated by CO chemisorption.*
[b] *The catalyst was prepared by H_2 reduction at 673 K for 2 hours after H_2PtCl_6 impregnation on γ-Al_2O_3 (4 mass % Pt).*
ND = not determined

to 90 times higher than TOF on the platinum nanoparticles (~ 20 Å) in FSM-16 (28 Å) (29). XPS and EXAFS data suggest that the unusually high TOF for the platinum nanowires may be linked to the different morphology and to a larger interaction (or contact) with the acidic surfaces of FSM-16 channels, resulting in a bigger electron deficiency than for FSM-16-encapsulated platinum nanoparticles.

The NO + CO Reaction

The Pt_9 and Pt_{12} carbonyl cluster dianions in NaY microcavities exhibit 10 to 15 times higher catalytic activity for NO reduction with CO to N_2 and N_2O at lower temperatures (300 to 473 K) (19, 20), compared to conventional Pt/γ-Al_2O_3 catalyst.

$$\left.\begin{array}{l} 2NO + CO \rightarrow N_2O + CO_2 \\ N_2O + CO \rightarrow N_2 + CO_2 \end{array}\right\} 2NO + 2CO \rightarrow N_2 + 2CO_2$$

When $[Pt_{12}(CO)_{24}]^{2-}$/NaY is exposed to NO (150 torr), *in situ* FTIR studies show that NO breaks the intra- and intertrigonal Pt-Pt bonds on the Pt_{12} carbonyl cluster – even at 298 K – to give a trigonal intermediate "$Pt_3(CO)_6$" and PtO(CO) during formation of N_2 (N_2O) and CO_2. Furthermore, $[Pt_{12}(CO)_{24}]^{2-}$ can be reversibly regenerated from platinum carbonyl fragments, such as "$Pt_3(CO)_6$" and PtO(CO), inside NaY by reaction with CO and water at 300 to 353 K to produce CO_2. *In situ* FTIR and mass spectrometry studies suggest that NO reduction with CO proceeds catalytically to give N_2/N_2O and CO_2 through redox cycles of cluster-breaking-regeneration ($Pt_{12} \leftrightarrow Pt_3 + Pt_9$) under the NO + CO atmosphere. In fact, the framework of the Pt_{12} clusters in NaY is apparently retained under the stationary reaction.

CO Hydrogenation to Alcohols

Hydroformylations of ethene and propene and CO hydrogenation were conducted at 373 to 453 K on $[Rh_6]$/NaY and RhFe/NaY (33, 34). Acetaldehyde was selectively obtained as the hydroformylation product on $[Rh_6]$/NaY, while with RhFe/NaY higher activities and selectivities for alcohols were obtained. In particular with RhFe/NaX, selectivities of close to 83 mol% for linear alcohol were obtained in propene hydroformylation, perhaps due to being confined in the basic NaX pores.

A reduced sample of $[Rh_6]+[Fe_3]$/NaY was catalytically active for the hydroformylation of ethene and propene with almost the same specific rates and selectivities as those obtained on $[Rh_6]$/NaY, but there were no RhFe bimetallic promotion sites in the reaction. By contrast, bimetallic RhFe/NaY (and RhFe/NaX) provided a good yield of oxygenates, mainly ethanol and methanol, and decreased the hydrocarbon content in the CO + H_2 reaction at 623 K (33, 35). In fact, $[Rh_6]$/NaY and $[Rh_6]+[Fe_3]$/NaY preferentially formed

methane and higher hydrocarbons with a minor yield of acetaldehyde. The results are accounted for by adjacent RhFe bimetal assemblies being active sites for the olefin hydroformylation and the CO + H_2 reaction to synthesise alcohols. It has been suggested that a two-site CO activation by bimetal clusters (for example, RhFe, RhCo and RuCo) on silica and alumina is responsible for the enhanced migratory insertion of CO into M-alkyl and M-H bonds (M is metal) to produce oxygenates from olefin carbonylation and CO hydrogenation, respectively (34).

Alkane Hydrogenolysis on RhIr Alloy Clusters in NaY

The hydrogenolyses of *n*-butane and ethane and benzene hydrogenation were used as probe reactions of RhIr alloy clusters prepared from $[Rh_{6-x}Ir_x(CO)_{16}]$ in NaY pores (11–13). A dramatic decrease in hydrogenolysis activity, by four orders of magnitude, across all the RhIr bimetallic clusters was observed as the number of iridium atoms in the rhodium assemblies was increased; the activity for benzene hydrogenation increased slightly. This remarkable suppression of activity was interpreted in terms of the rhodium assembly-size effect (rhodium clusters were broken by a modest iridium atom), and of decreasing electron deficiency of the rhodium-rich bimetal clusters in NaY. Alkane hydrogenolysis is classed as a "structure-sensitive" reaction in which relatively large ensembles of metal atoms are required to break the multi-bonds of reactant molecules such as CO, N_2 and alkanes. By contrast, benzene hydrogenation has a different response (it is structure-insensitive) to the metal composition of RhIr clusters in NaY. These results demonstrate the important advantage of the "ship-in-bottle" technique for putting bimetallic clusters in micropores, giving an isolated site model for heterogeneous catalysis (3, 5).

Conclusions

Novel templating syntheses of nanomaterials using inorganic micro- and mesoporous cages and channels for the tailored design of platinum metals catalysts have been discussed. Extending these techniques could result in nanotechnology being used to produce nanoparticle alloy catalysts – of PtRe, PtIr and PtCo, for example, – in zeolites and textured carbon, with higher performances for oil refining and for hydrogen-powered fuel cells. New ways of synthesising fine chemicals, using the spatially confined chiral space of mesoporous material, implanted with platinum metals clusters, may also result. The novel "ship-in-bottle" nanotechnology can provide spatial ordering and alignment of nanoparticles and nanowires of metals and semiconductors, and for photosensitisers for microdevices, for electronics, magnetics and non-linear optics. Further research would help to explain the dependence of cluster catalysis and catalyst stability on structure and morphology and explain the micro-mechanisms of cluster-sintering and metal-support interactions.

Acknowledgements

Dr A. Fukuoka and T. Shido of C.R.C., Hokkaido University are thanked for their expertise and crucial contributions associated with this subject.

References

1 (a) B. C. Gates, "Catalyst Design", ed. L. L. Hegedus, Wiley, Chichester, 1987, p. 71; (b) B. C. Gates, "Metal Clusters", ed. M. Moskovits, Wiley, New York, 1986, p. 283

2 "Surface Organometallic Chemistry", eds. J. M. Basset and R. Wymann, NATO Ser., Vol. **231**, 1988, pp. 75–90

3 (a) M. Ichikawa, *Adv. Catal.*, 1992, **38**, 283; (b) M. Ichikawa, *CHEMTECH*, 1982, **12**, 674; (c) M. Ichikawa, 'Dynamic Aspects in Heterogeneous Catalysis' in "Dynamic Processes on Solid Surfaces", ed. K. Tamaru, Plenum Pub., 1994, pp. 149–216

4 H. Vahrenkamp, *Adv. Organometal. Chem.*, 1983, **22**, 674

5 (a) M. Ichikawa, 'Chemisorption and Reactivity on Supported Clusters and Thin Films', in "Towards an Understanding on Microscopic Processes in Catalysis", eds. R. M. Lambert and G. G. Pacchioni, Kluwer Pub., Dordrecht, 1997, pp. 153–192; (b) M. Ichikawa, *Polyhedron*, 1988, **7**, 2351

6 S. Kawi and B. C. Gates, "Clusters and Colloids - From Theory to Application", ed. G. Schmid, VCH Publisher, New York, 1994, pp. 300–372

7 (a) T. M. Maschmeyer, F. Rey, G. Sankar and J. M. Thomas, *Nature*, 1995, **378**, 159; (b) G. A. Ozin and S. Ozkar, *Chem. Mater.*, 1992, **4**, 511; (c) G. Schmidt, *Struct. Bonding (Berlin)*, 1985, **62**, 51; *Mater. Chem. Phys.*, 1991, **29**, 133

8 Y. C. Xie and Y. Q. Tang, *Adv. Catal.*, 1990, **37**, 1

9 M. Ichikawa, L. F. Rao, N. Kosugi and A. Fukuoka, *J. Chem. Soc., Faraday Diss.*, 1989, **87**, 232

10 L. F. Rao, A. Fukuoka, N. Kosugi, H. Kuroda and M. Ichikawa, *J. Phys. Chem.*, 1990, **94**, 5317

11 S. Martinengo, P. Chini, G. Giordano, V. G. Albano and G. Cianti, *J. Organomet. Chem.*, 1975, **88**, 375

12 M. Ichikawa, L. F. Rao, T. Kimura and A. Fukuoka, *J. Mol. Catal.*, 1990, **62**, 15

13 (a) S. Kawi and B. C. Gates, *J. Chem. Soc., Chem. Commun.*, 1991, 904; (b) S. Kawi, J. R. Chang and B. C. Gates, *J. Am. Chem. Soc.*, 1993, **115**, 4830

14 (a) L. L. Sheu, H. Knozinger and W. M. H. Sachtler, *Catal. Lett.*, 1989, **2**, 35; (b) *J. Am. Chem. Soc.*, 1989, **111**, 8125

15 (a) G. C. Chen, T. Shido and M. Ichikawa, *J. Phys. Chem.*, 1996, **100**, 16947; (b) M. Ichikawa, A. M. Liu, G. S. Shen and T. Shido, *Top. Catal.*, 1995, **2**, 141

16 (a) G. C. Shen, A. Liu and M. Ichikawa, *J. Chem. Soc., Faraday Trans.*, 1998, **94**, 1353; (b) A.-M. Liu, T. Shido and M. Ichikawa, *J. Chem. Soc., Chem. Commun.*, 1995, 507

17 (a) G. Shen, T. Shido and M. Ichikawa, *J. Phys. Chem.*, 1996, **100**, 16947; (b) J. G. C. Shen, A. Liu and M. Ichikawa, *J. Phys. Chem. B*, 1998, **102**, 7782

18 A. De Mallmann and D. Barthorneuf, *Catal. Lett.*, 1990, **5**, 293

19 G. J. Li, T. Fujimoto, A. Fukuoka and M. Ichikawa, *J. Chem. Soc., Chem. Commun.*, 1991, 1337

20 G. J. Li, T. Fujimoto, A. Fukuoka and M. Ichikawa, *Catal. Lett.*, 1992, **12**, 171

21 J. S. Beck, J. C. Sartuli, W. J. Roth, C. T. Leonowicz and S. K. Kreag, *J. Am. Chem. Soc.*, 1992, **114**, 10843

22 T. Yanagisawa, T. Shimizu, K. Kuroda and C. Kato, *Bull. Chem. Soc. Jpn.*, 1990, **62**, 763; Y. Inagaki, Y. Fukushima and K. Kuroda, *J. Chem. Soc., Chem. Commun.*, 1993, 680

23 T. Yamamoto, T. Shido, S. Inagaki, Y. Fukushima and M. Ichikawa, *J. Am. Chem. Soc.*, 1996, **118**, 5810

24 T. Yamamoto, T. Shido, S. Inagaki, Y. Fukushima and M. Ichikawa, *J. Phys. Chem. B*, 1998, **102**, 3866

25 A. Fukuoka, L. F. Rao, N. Kosugi, H. Kuroda and M. Ichikawa, *Appl. Catal.*, 1988, **50**, 295

26 (a) D. S. Shephard, T. Maschmeyer, B. F. G. Johnson, J. M. Thomas, G. Sankar, D. Ozkaya, W. Zhou, R. D. Oldroyd and R. G. Bell, *Angew. Chem., Int. Ed. Engl.*, 1997, **36**, 2242; (b) D. S. Shephard, T. Maschmeyer, G. Sankar, J. M. Thomas, D. Ozkaya, B. F. G. Johnson, R. Raja, R. D. Oldroyd and R. G. Bell, *Chem. Eur. J.*, 1998, **4**, 1214

27 A. Fukuoka, T. Kimura, N. Kosugi, H. Kuroda, Y. Minai, Y. Sasaki, T. Tominaga and M. Ichikawa, *J. Catal.*, 1990, **126**, 434

28 M. Sasaki, M. Osada, N. Higashimoto, S. Inagaki, Y. Fukushima, A. Fukuoka and M. Ichikawa, *Micro. Mesoporous Mater.*, 1998, **21**, 597

29 M. Sasaki, M. Osada, N. Higashimoto, T. Yamamoto, A. Fukuoka and M. Ichikawa, *J. Mol. Catal., A*, 1999, **141**, 223

30 C. H. Ko and R. Ryoo, *Chem. Commun.*, 1996, 2467

31 R. Wang, T. Fujimoto, T. Shido and M. Ichikawa, *J. Chem. Soc., Chem. Commun.*, 1992, 962

32 A. Fukuoka, T. Kimura and M. Ichikawa, *J. Chem. Soc., Chem. Commun.*, 1988, 428

33 M. Ichikawa, A. Fukuoka and T. Kimura, Proc. Int. Congr. Catal., 9th, 1988, Vol. 1, 569

34 (a) M. Ichikawa, A. J. Lang, D. F. Shriver and W. M. H. Sachtler, *J. Am. Chem. Soc.*, 1985, **107**, (24), 7216; (b) W. M. H. Sachtler and M. Ichikawa, *J. Phys. Chem.*, 1986, **90**, 475; (c) A. Fukuoka, M. Ichikawa, J. A. Hriljac and D. F. Shriver, *Inorg. Chem.*, 1987, **26**, 3643

35 L. F. Rao, A. Fukuoka and M. Ichikawa, *J. Chem. Soc., Chem. Commun.*, 1988, 458; L. F. Rao and A. Fukuoka, in "Catalytic Science and Technology.", Proc. 1st Int. Conf. Adv. Catal. Sci. Technol., Tokyo, 1990, Kodansha-VCH, Vol. 1, 1991, 111–116

The Author

Professor Masaru Ichikawa is head of the Laboratory of Advanced Catalyst Design, Catalysis Research Center, Hokkaido University, Japan. His main interests are in the molecular design of heterogeneous catalysts using metal cluser complexes, the "ship-in-bottle" synthesis of metal/alloy clusters and nanowires in micro/mesoporous spaces and their catalysis for C1 reactions, and methane conversion to benzene and hydrogen.

Colloidal Gold/Platinum Building Blocks

There is current interest in producing large anisotropic molecular structures which can self assemble and take part in catalytic reactions. One way of doing this would be to use anisotropic nanoparticles as building blocks.

Scientists at The Pennsylvania State University have recently developed a method to produce anisotropic multirods of colloidal particles with controllable surface chemistry via spacial self assembled monolayers (SAMs) (B. R. Martin, D. J. Dermody, B. D. Reiss, M. Fang, L. A. Lyon, M. J. Natan and T. E. Mallouk, *Adv. Mater.*, 1999, **11**, (12), 1021–1025). Striped nanorods of Au/Pt and Au/Pt/Au colloidal particles were sequentially electroplated from Au and Pt plating solutions inside a porous template membrane in an ultrasonication bath, which together with a temperature control bath, aided the mass transport of ions and gases through the membrane. Rods 200–300 nm long were produced. Attaching SAMs with appropriate tail groups to the metals enhances the suspension of the rods and allows their manipulation. The Au and Pt in the rods were derivatised with 1-butaneisocyanide with thiol groups, which are attracted to Au, 2-mercaptoethylamine and finally Rhodamine-B isothiocyanate. Fluorescence microscopy showed that only the Au rods fluoresce.

Thus, the surface chemistry of these single multimetal colloidal particles is controllable via orthogonal self assembled molecules and the chemical manipulation of these building blocks represents a first step towards anisotropic mesoscale assembly and possible electrical and optical applications.